International Journal of Applied Earth Observation and Geoinformation 13 (2011) 668–675

Contents lists available at ScienceDirect

International Journal of Applied Earth Observation and Geoinformation

journal homepage: www.elsevier.com/locate/jag

Empirical test of the spectral invariants theory using imaging spectroscopy data from a coniferous forest

Petr Lukeš[a,*], Miina Rautiainen[b], Pauline Stenberg[b], Zbyněk Malenovský[c]

[a] Global Change Research Centre, Academy of Sciences of the Czech Republic, v.v.i., Bělidla 986/4a, Brno 603 00, Czech Republic
[b] Department of Forest Sciences, PO BOX 27, University of Helsinki, FI-00014, Finland
[c] Remote Sensing Laboratories, Department of Geography, University of Zürich, Winterthurstr. 190, CH-8057 Zürich, Switzerland

ARTICLE INFO

Article history:
Received 26 September 2010
Accepted 12 April 2011

Keywords:
Recollision probability
Escape factor
Needle albedo
CHRIS PROBA
AISA

ABSTRACT

The spectral invariants theory presents an alternative approach for modeling canopy scattering in remote sensing applications. The theory is particularly appealing in the case of coniferous forests, which typically display grouped structures and require computationally intensive calculation to account for the geometric arrangement of their canopies. However, the validity of the spectral invariants theory should be tested with empirical data sets from different vegetation types. In this paper, we evaluate a method to retrieve two canopy spectral invariants, the recollision probability and the escape factor, for a coniferous forest using imaging spectroscopy data from multiangular CHRIS PROBA and NADIR-view AISA Eagle sensors. Our results indicated that in coniferous canopies the spectral invariants theory performs well in the near infrared spectral range. In the visible range, on the other hand, the spectral invariants theory may not be useful. Secondly, our study suggested that retrieval of the escape factor could be used as a new method to describe the BRDF of a canopy.

1. Introduction

Three-dimensional (3D) radiative transfer models are efficient tool in simulating the radiation reflected from a highly structured forest canopy. However, such models require detailed spatial and structural input of vegetation canopies. Thus, 3D radiative transfer models are difficult to parameterize in practical remote sensing applications. As a solution to this problem, Widlowski et al. (2007) suggested that future investigations should look into by how much results of radiative transfer simulations vary when carried out for canopy representations with a progressively increasing degree of structural complexity. Currently, the use of one-dimensional (1D) models is still a relatively popular alternative (e.g. Huang et al., 2008), even though it limits the possibilities of taking full advantage of modern multiangular and imaging spectroscopy data (Schaepman et al., 2009). An ideal solution would comprise a radiative transfer approach as realistic as a 3D model but as simple as a 1D model.

The novel concept of canopy spectral invariants (Knyazhikin et al., 2011; Huang et al., 2007) may present an alternative approach for modeling canopy scattering. The spectral invariants theory states that the canopy albedo at any specific wavelength is related to the leaf albedo at the same wavelength through photon recollision probability, p. The "photon recollision probability" can be interpreted as the probability that a photon scattered from a leaf in the canopy will interact within the canopy again (Smolander and Stenberg, 2005). The escape factor, in turn, describes the probability of escape into a particular view angle. In other words, the probabilities for photon–vegetation interactions in a canopy are determined by the geometric structure of the canopy rather than wavelength. Thus, the probabilities determining the interactions are called "spectral invariants". Furthermore, spectral invariants enable calculation of all components related to the shortwave radiation budget of a canopy (for any given wavelength) if the leaf albedo at the same wavelength is known (Smolander and Stenberg, 2005).

The concept of spectral invariants would remain purely theoretical if it were not linked to measurable properties of real-world vegetation. Recently, Stenberg (2007) showed that it is possible to estimate an average photon recollision probability value for a forest canopy from field measurements carried out with the LAI-2000 Plant Canopy Analyzer or a hemispherical digital camera. Stenberg derived an analytical formula by which p can be calculated from

* Corresponding author.
E-mail addresses: lukes.p@czechglobe.cz (P. Lukeš), miina.rautiainen@helsinki.fi (M. Rautiainen), pauline.stenberg@helsinki.fi (P. Stenberg), zbynek.malenovsky@geo.uzh.ch (Z. Malenovský).

0303-2434/$ – see front matter © 2011 Elsevier B.V. All rights reserved.
doi:10.1016/j.jag.2011.04.003

canopy gap fraction data. At the same time, Schull et al. (2007), in turn, put forth an algorithm for estimating the photon recollision probability and escape factor for vegetation canopies from imaging spectroscopy data.

The value of the spectral invariants theory for remote sensing applications is based on the observation that at least two spectral invariants, canopy interceptance and the recollision and escape probabilities are potentially sensitive to important structural features of a vegetation canopy (Schull et al., 2011). According to the current understanding, the low NIR reflectances in coniferous areas are mainly due to within-shoot scattering, and can be efficiently modeled using photon recollision probability in radiative transfer models (Rautiainen and Stenberg, 2005; Smolander and Stenberg, 2005). In addition, spectral invariants can be linked to easily conceivable forest variables such as leaf area index and crown shape (Schull et al., 2007; Stenberg, 2007; Rautiainen et al., 2009).

Theoretical modeling studies have also indicated that spectral invariants are coherent with physically based canopy reflectance models. Structure makes canopies more efficient absorbers of the collided radiation, which results in higher photon recollision probabilities and changes the escaped factors for different scattering orders (Mõttus et al., 2007; Mõttus, 2007). Furthermore, the fraction of radiation scattered upwards by a canopy can be accurately modeled using a simple parameterization based on a diffuse photon recollision probability (Mõttus and Stenberg, 2008). Spectral invariants may also offer a physically meaningful measure of canopy structure over a wide range of scales (Lewis and Disney, 2007), and thus, provide a method for remote sensing of biophysical canopy variables and separation of tree species (Schull et al., 2011). For example, Ganguly et al. (2008a,b) have successfully applied the spectral invariants theory to develop a physically based approach for deriving global LAI and fraction of absorbed PAR (FPAR) products from the Advanced Very High Resolution Radiometer (AVHRR) data.

The spectral invariants theory is particularly appealing in the case of coniferous canopies, which typically display grouped structures and require a computationally efficient way to describe the geometric arrangement of their canopies. Before further conclusions are drawn concerning the feasibility and validity of the spectral invariants theory, the methods for estimating spectral invariants must be tested with empirical data sets from different vegetation types. In this paper, we (1) evaluate a method to retrieve canopy spectral invariants (photon recollision probability, escape factor) for a coniferous forest from CHRIS PROBA and AISA imaging spectroscopy data, (2) study the effect of view angle on the retrieved spectral invariants and, finally, (3) discuss the limitations and future potential in estimating spectral invariants from imaging spectroscopy data.

2. Experiment research site and input ground measurements and remote sensing data

2.1. Research site

The "Bílý Kříž" research site is located in the Moravian-Silesian Beskydy Mountains (18.54°E, 49.50°N, mean elevation of 894 m a.s.l.) in the Czech Republic. The climate is moderately cold, damp and rainy-rich with ten-year average annual air temperature of 6.7 ± 1.2 °C (period 1998–2007), average humidity of 82 ± 4%, and average annual rainfall of 1374 ± 186 mm (Kratochvilová et al., 1989). The research site is part of the FLUXNET international network for measuring CO_2 fluxes using the Eddy-covariance technique (Oak Ridge National Laboratory Distributed Active Archive Center, 2005).

In this study, we used an intensively studied 29-year old coniferous forest in the "Bílý Kříž" area. Our study site consists of regularly planted Norway spruce (*Picea abies* (L.) Karst.) forest (an area of 11,560 m^2). The forest stand grows on a moderate slope of 13.42° with a southern aspect. In 2006, the stand density (for our study area) was 1430 stems ha^{-1}, with an average tree height of 11.6 m and an average diameter at breast height (DBH) of 14.3 cm. The canopy was closed (canopy cover about 80%), i.e. understory vegetation and bare soil background was almost not visible to air- or satellite-borne remote sensing instruments. The data used in this study were collected during a field and flight campaign organized in September 2006.

2.2. Needle albedo measurement

Measurements of leaf albedo are required to retrieve spectral invariants from imaging spectroscopy data. Ten sample Norway spruces were randomly selected at the study site, and twelve needle samples per tree (120 needle samples in total) were collected and measured for leaf optical properties within one week after the airborne and space-borne image data acquisitions. The needle-sampling scheme was designed to capture the full variability of needle optical properties within a crown vertical profile, resulting from presence of several needle generations and decreasing intensity of irradiation. Therefore, needles of the last four needle age-classes (C: current year, C+1: 1 year old, C+2: 2 years old, and C++: 3 years and older needles) were collected from three branches: (i) sun exposed (*E*: branches that are never shaded by neighboring phytoelements), (ii) transitional (*T*: branches that are shaded from direct sun irradiation for a fraction of the day), and (iii) shaded (*S*: branches that are in diffuse illumination environment only). The needles, sampled from south-facing side of crown, were placed in zip-lock plastic bags with wet paper pulp and kept in a dark cooler (about 8 °C) of the field laboratory until their processing (max. 6 h).

The needle directional-hemispherical reflectance and transmittance values between 400 and 1600 nm were measured in anoptical integrating sphere Li-1800-12 (Li-Cor, Inc., USA) coupled with a FieldSpec-3 (ASD, Inc., USA) field/laboratory spectroradiometer. 150 scans were averaged per sample. The leaf optical properties were measured and computed according to the methodology and equations originally proposed by Daughtry et al. (1989) and extended by Mesarch et al. (1999). The step-by-step protocol used in this study for measurement of Norway spruce needle samples is described in detail in Malenovský et al. (2006). Directional-hemispherical reflectance (ρ) and transmittance (τ) of sample needles was computed according to the following equations:

$$\rho = \frac{(R_{\mathrm{TOTAL}} - \mathrm{STR}/\mathrm{REF} - \mathrm{STR})}{(1 - \mathrm{GF}_R)} \quad (1)$$

$$\tau = \left[\left(\frac{T_{\mathrm{TOTAL}}}{\mathrm{REF} - \mathrm{STR}}\right) - (\rho_W \mathrm{GF}_T)\right] \frac{1}{(1 - \mathrm{GF}_T)} \quad (2)$$

where R_{TOTAL} is the flux of radiation reflected from the sample in reflectance mode, STR is the flux of stray light radiation, REF is the flux of radiation reflected from a $BaSO_4$ reference standard in reference mode, GF_R is the gap fraction of the sample in reflectance mode, T_{TOTAL} is the flux of radiation transmitted through the sample in transmittance mode, ρ_W is the reflectance of integrating sphere wall, and GF_T is the gap fraction of the sample in transmittance mode (for more details see Malenovský et al., 2006). The resulting spectral library was quality checked, and the erroneous spectral signatures that occurred in case of extremely short and/or strongly arc-shaped needles were excluded from the final data set.

High variability in leaf optical properties can be observed within needle age-classes and irradiation conditions, particularly in green spectral region between 495 and 690 nm and longer wavelengths

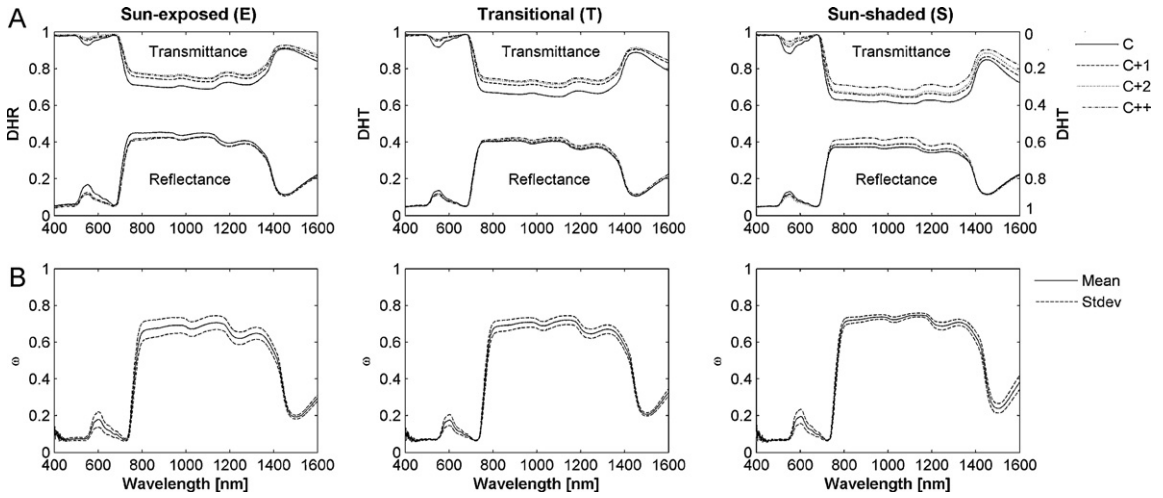

Fig. 1. (a) Variations in needle optical properties (reflectance and transmittance) measured for 10 Norway spruce trees at different crown positions and needle age-classes (*E*: sun-exposed, *T*: transitional, and *S*: sun-shaded part of the crown). The spectral range and position of CHRIS straight line) and AISA (dashed) bands are marked. Note the significant differences of DHR and DHT in VIS (395–690 nm) and NIR + SWIR wavelengths (740–1600 nm). (b) Mean needle albedo and its standard deviation at different crown positions.

Table 1
Weights used to derive mean ω_L for Norway spruce trees for different crown positions (*E*: sun-exposed, *T*: transitional, *S*: sun-shaded) and needle age classes (C – one year old needles, C+1 – two years old needles, C++ – mixed sample of older needles). The highest weights were placed on the exposed (*E*) part of the crown. The shaded part of crowns (*S*) played only minor role in calculation of crown mean ω_L. The exposed (*E*) part captured most of the incoming PAR.

	E	*T*	*S*
C	0.22	0.06	0.0005
C+1	0.22	0.08	0.0095
C++	0.09	0.3	0.02

between 740 and 1600 nm (Fig. 1a). The needle albedo values (ω), computed assume of $\rho + \tau$ and averaged through the age-classes of each irradiation condition, are similar in the visible wavelengths (Fig. 1b). When compared to the sun-exposed needles, the albedo in NIR of the sun-shaded needles is higher with a low standard deviation. Differences in the NIR region (Fig. 1b) are driven mainly by variability of transmittance values, originating from changes in needle anatomy and differences in needle thickness and shape. Considering the high structural complexity of coniferous forests and the subsequent heterogeneous irradiation conditions, a simple arithmetic mean of all needle albedo measurements would result in a non-representative estimate. To obtain a representative leaf albebo (ω_L) of the whole forest test site, i.e. to properly take into account the variability introduced by different needle age-classes and irradiation conditions (Fig. 1), the measurements were integrated using a weighted average. A leaf albedo for each tree crown was computed as the weighted mean of measured leaf ρ and τ, combining two weights: (1) a weight based on the amount of needle age-class biomass, and (2) a weight resulting from vertical light extinction within the crown (Table 1).

The biomass distribution of needle-age classes was measured destructively from six representative sample trees of the study forest in 2007. Six branches were taken per tree in different vertical irradiation conditions. Branches up to the 6th whorl from top were assigned to sun-exposed (*E*), from 7th to 10th to transitional (*T*), and the lower (up to the 18th whorl) to sun-shaded (*S*) part of crown. Dry needle biomass weight per needle age-class was expressed as a percentage of total needle area within crown (results not shown). The vertical weights were derived from measurements of light extinction within a crown profile measured with the CANFIB device (ISBE AS CR, Czech Republic). CANFIB consists

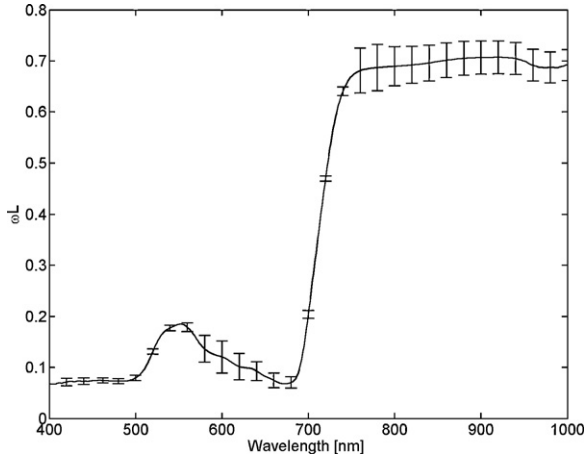

Fig. 2. Mean ω_L computed according to the spectral characteristics of the AISA Eagle and CHRIS (vertical line) sensors. The response function of the CHRIS sensor was used to calculate its specific ω_L. The spectral region of 500–994 nm (full-width-half-maximum of 3.3 nm, 259 image bands) was used as the AISA-specific ω_L.

of a cosine light diffuser and sensors measuring incoming photosynthetically active radiation (PAR ~ 400–700 nm). The CANFIB measurements were automatically collected at several whorls and shoot age-classes, following the sampling scheme of needle optical properties (Urban et al., 2007). The relative PAR, expressed as a fraction of the above canopy PAR in each monitored crown level, was used as the vertical weight. Means of ρ and τ for the ten sampled Norway spruce crowns weighted by combined coefficients in Table 1 were arithmetically averaged to produce a single reference ω_L of the whole study forest. Finally, the ω_L values were convoluted according to spectral specifications (i.e., spectral resolution, sampling, and full-width-half-maximum, FWHM) of the AISA and CHRIS sensors (Fig. 2).

2.3. Ground measurements of LAI and estimation of photon recollision probability

An effective leaf area index (LAI_e) of a 50 m × 50 m plot located within our study site was measured with one unit of the LAI-2000 Plant Canopy Analyzer (Li-Cor, Inc., USA). The measurements were made in diffuse radiation conditions shortly before sunrise or after

Table 2
CHRIS/PROBA multiangular data acquired in September 2006 for the Bílý Kříž test site.

Viewing angle	True OZA [°]		
	12.9.2006	13.9.2006	22.9.2006
NADIR	16.04	7.03	14.02
36°	34.48	32.55	32.95
−36°	38.14	37.31	37.85
55°	54.94	54.47	53.82
−55°	57.52	56.09	56.37
Solar zenith angle	46.5	46.6	49.7
Fly-by time [UTC]	9:51	10:02	10:06

dusk in September 2006. A total of 61 points were measured in the plot: the main measurement grid consisted of 6 × 6 regularly placed points (with distance of 10 m between points) and the secondary grid consisted of 5 × 5 points (placed inside the main grid and shifted by 5 m in both axes). Since clumping at small spatial scales (e.g. needles into shoots) is not accounted for in the standard LAI estimates provided by the LAI-2000 PCA instrument, a correction for the clumping of needles into shoots was done separately. Correction from effective (LAI_{eff}) to true leaf area index (LAI_{true}) was carried out using a site-specific correction factor (1.6, which corrects both for shoot-scale clumping and also presence of woody biomass), derived with destructive sampling from trees growing at the study forest stand (Pokorný, 2002). The correction factor can be considered robust because the same stand was used for indirect estimation of LAI_{eff}. The true LAI (LAI_{true}) within the study site was estimated to be 7.7 m^2 m^{-2} (Pokorný et al., 2008).

Next, an average photon recollision probability (p) of the study forest was estimated from measured canopy uncollided transmittances (i.e., canopy gap fractions or canopy diffuse non-interceptance DIFN measured with the LAI-2000 PCA instrument) in different view directions using the method proposed by Stenberg (2007):

$$\hat{p} = 1 - \frac{1 - \mathrm{DIFN}}{\mathrm{LAI_{true}}} \tag{3}$$

Stenberg (2007) showed that the average p is directly related to the canopy interceptance per unit needle area, where canopy interceptance (1 − DIFN) refers to the portion of incoming isotropic radiation that is intercepted by the leaves or needles in a canopy. This results in a recollision probability that is averaged over all points on the canopy leaf (needle) area. The average p for our study site, in this paper called the "ground reference p", was estimated to be 0.88 with a standard deviation of 0.02.

2.4. Remote sensing data

Two independent remote sensing datasets were used in this study: (1) airborne imaging spectroscopy data of very high spectral and spatial resolution from the AISA Eagle sensor and (2) satellite multiangular imaging spectroscopy data of high spatial resolution provided by the CHRIS sensor on board the PROBA space-borne platform (Table 2).

Airborne imaging spectroscopy reflectance data were acquired by the push broom imaging spectrometer AISA Eagle (Specim, Finland) on 14th of September 2006, 10-00 UTC. Images of 260 spectral bands between 397 and 994 nm and mean full-width-half-maximum (FWHM) of 3.3 nm were collected at a ground spatial resolution of 6 m. All image bands were georeferenced using the in-flight navigation INS/GPS data, transformed into at-sensor radiance with the sensor-specific calibration files, and atmospherically corrected using the atmospheric radiative transfer model ATCOR4 (ReSe, UZH, Switzerland). The final georeferencing accuracy of 20.8 m (3.5 pixels) was assessed using several GCPs derived from ancillary aerial ortho-photo maps. The quality of the radiometric and atmospheric corrections was verified against in situ measured ground reflectance of natural and artificial homogeneous surfaces. The observed mean difference in reflectance values was equal to 1.8% at 550 nm, and to 2.6% at 850 nm.

Compact High Resolution Imaging Spectrometer (CHRIS) on board the PRoject for On Board Autonomy 1 (PROBA-1) satellite represents one of the first space-borne programmable multi-angular true imaging spectroradiometers. CHRIS has a unique capability to acquire imaging spectroscopy data of a nominal spatial resolution of 17-34 m (image swath of 13 km) in 5 different viewing angles (±0°, ±36°, and ±55°). Three close-in-time CHRIS scenes were acquired over Bílý Kříž test site during September 2006. Unfortunately, the most oblique backward scattering image (−55°) did not cover our study site and therefore was not available. The images were acquired in CHRIS mode 4, designed particularly for chlorophyll content (C_{a+b}) analyses. Mode 4 has 18 channels located in the visible and near-infrared spectral range of 485–800 nm. Bandwidth ranges from 5.8 nm in the near-infrared (NIR) to 14.9 nm in the visible (VIS) region. The solar zenith angle and fly-by times were for all three scenes relatively similar (see Table 2). Basic radiometric corrections (vertical stripping and drop-outs) and atmospheric corrections were performed with the BEAM software (ESA) using a publicly available CHRIS toolbox. Since our study site is situated on a relatively small slope with south orientation, geometric effects of terrain play only a minor role. Therefore, no geometric correction was required. The CHRIS scene from 12th of September 2006, independently atmospherically corrected in ATCOR2/3 software (ReSe, UZH, Switzerland), was used to evaluate the performance of atmospheric corrections in BEAM, showing reciprocal root-mean-square-error (RMSE) of negligible magnitude (from 0.41% for NADIR up to 1.26% for −55° viewing angle).

2.5. Retrieval of spectral invariants from remote sensing data

According to the spectral invariants theory (i.e. assuming p to remain constant in successive interactions), the bidirectional reflectance factor (BRF) of a canopy bounded underneath by a non-reflecting surface can be expressed as (Rautiainen and Stenberg, 2005):

$$\mathrm{BRF}(\Omega_S, \Omega_V) = \frac{i\Omega_S f(\Omega_V)((1-p)\omega_L)}{1 - p\omega_L} \tag{4}$$

where Ω_S and Ω_V denote the directions of incident radiation (sun) and view, $i(\Omega_S)$ is canopy interceptance and $f(\Omega_V)$ describes the directional distribution of the canopy scattering normalized by that of a Lambertian surface.

Schull et al. (2007) showed that according to Eq. (4), the ratio of canopy BRF to ω_L is linearly related to canopy BRF, and the slope and intercept of the obtained line correspond to the photon recollision probability (p) and the directional escape factor ($e(\Omega_S\Omega_V) = i(\Omega_S)f(\Omega_V)(1-p)$):

$$\frac{\mathrm{BRF}(\Omega_S, \Omega_V)}{p\omega_L} = p \times \mathrm{BRF}(\Omega_S, \Omega_V) + e(\Omega_S, \Omega_V) \tag{5}$$

The method by Schull et al. (2007) was applied to the remote sensing data from Bílý Kříž. Because the spruce canopy in our study forest is very dense and closed (mean canopy closure about 80%), the assumption of "black soil" behind Eq. (5) was not considered to be a problem. Forest BRF's from the AISA Eagle and CHRIS scenes were extracted as a mean value of a rectangular region (size: 140 m × 85 m) over the study forest. We used the same mean needle albedos (ω_L) for all acquisition dates and angles (Fig. 2).

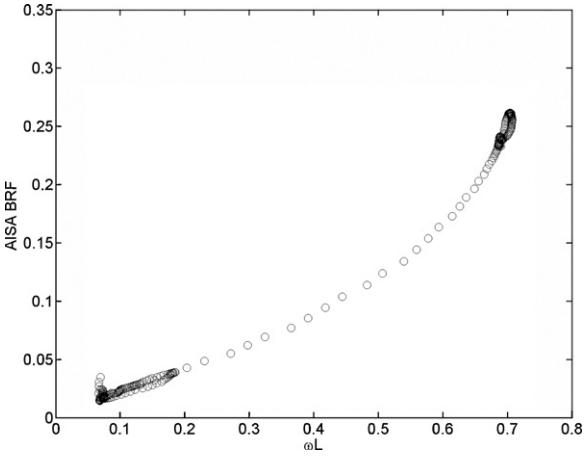

Fig. 3. AISA BRF as a function of needle albedo. Curvilinear relationship according to Eq. (2) was observed.

3. Results and discussion

3.1. Spectral invariants

BRF as a function of mean needle albedo (ω_L) showed a similar curvilinear relationship as predicted by Eq. (4) (Fig. 3). The curvature of the relationship is characterized by the p-value; the more non-linear is the relationship, the higher is p. However, the method proposed by Schull et al. (2007) for retrieving spectral invariants performed well only in the NIR domain and poorly in the VIS domain for the NADIR-view AISA image. A similar behavior was also observed in the original results by Schull et al. (2007). A non-linear, scattered relationship between BRF/ω_L and canopy BRF was observed for VIS wavelengths (500–707 nm), whereas a relatively linear relationship was noted for the NIR wavelengths (707–994 nm) (Fig. 4a). When both VIS and NIR domains (500–994 nm) were included in the regression analysis, the recollision probability p was 0.618 (i.e. slope of line) and the directional escape factor $e(\Omega_S,\Omega_V)$ was 0.199 (i.e. intercept of line). However, when only the NIR wavelengths (707–994 nm) were included, a near-perfect linear relationship was observed with a slope (p) of 0.868 and an intercept (e) of 0.139 (Fig. 4b). Similar scattered relationships between BRF/ω_L and canopy BRF were also observed in all view angles of the CHRIS images for VIS wavelengths (480–707 nm), creating a hockey stick-like curve shape (Fig. 5). Once again, when the spectral range was limited to wavelengths above 707 nm, a close to ideal linear relationship between canopy BRF/ω_L and BRF was observed for all viewing angles (Fig. 6). However, the retrieved values of the probability p frequently exceeded the theoretical upper limit (Table 3), indicating failure of the retrieval algorithm.

A possible explanation for the observed hockey stick-like behavior (Figs. 4a and 5) is that in the VIS the amount of reflected energy is low, and originates mainly from first-order scattering. The high absorption of incident radiation in VIS is caused by foliar pigments (e.g. chlorophylls a and b), which are driving factors of reflectance in the VIS region. The assumption of spectral invariance of p was invalid in the VIS domain, where plant biochemistry rather than canopy structure plays a major role. In the NIR domain, p exhibited a spectrally invariant behavior, but theoretically sound values ($p < 1$) were obtained only in the NADIR-viewing direction.

By theory, photon recollision probability p is independent of sun and view angle, in contrast to the directional escape factor $e(\Omega_S,\Omega_V)$. In the multi-angular CHRIS data set, forward-scattering directions (+36° and +55°) produced a slightly higher p than the NADIR data, and noticeably higher p than the backward-scattering direction (-36°). The retrieved values of the escape factor $e(\Omega_S,\Omega_V)$,

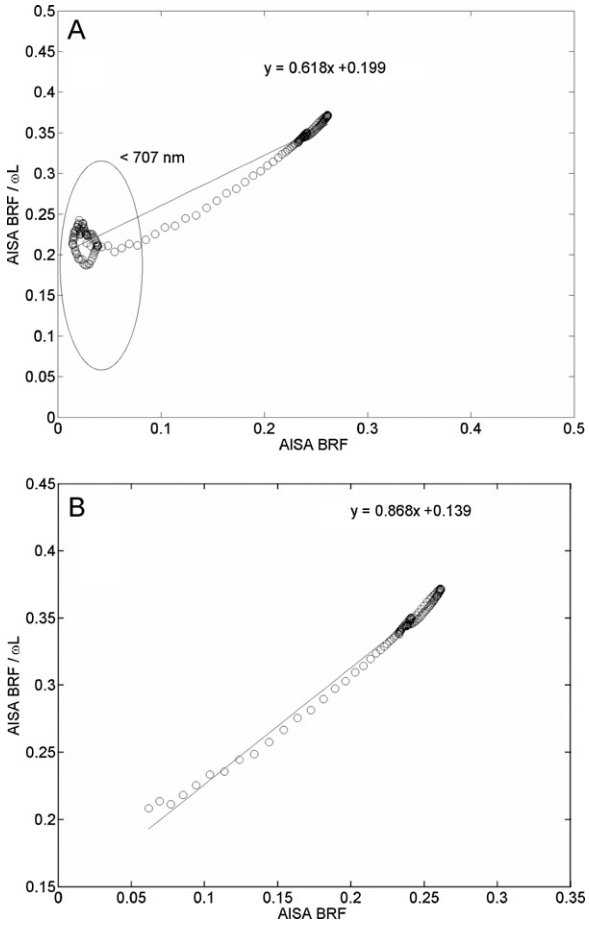

Fig. 4. AISA BRF/ω_L vs. AISA BRF relationship for (a) entire range of VNIR wavelengths (500–994). Recollision probability p is 0.503 and directional escape factor $e(\Omega_S\Omega_V)$ is 0.250. (b) NIR wavelengths (707–994 nm). Recollision probability p is 0.954 and directional escape factor $e(\Omega_S\Omega_V)$ is 0.144.

in turn, were the highest in the NADIR viewing direction. (Table 3 summarizes the regression equations.) In forward scattering directions, p was frequently beyond its physically meaningful range of 0–1, whereas in the NADIR direction the retrieved p was closest to our ground reference p. The observed angular dependency of p retrieved from the imaging spectroscopy data is in conflict with the spectral invariants theory, but may partly be a result of the coupling of p and $e(\Omega_S,\Omega_V)$ in the retrieval algorithm. Unrealistic values of p may also result from uncertainties of ω_L. The directional escape factor $e(\Omega_S,\Omega_V)$, on the other hand, should follow the bi-directional reflectance distribution function (BRDF) of vegetation, which is known to be a strong backward scatterer. Our results for the retrieval of $e(\Omega_S,\Omega_V)$ agreed with this expectation: the highest $e(\Omega_S,\Omega_V)$ were consistently observed in backward scattering −36° angles and a rapid drop in $e(\Omega_S,\Omega_V)$ was observed towards the forward scattering directions. However, correct interpretation of $e(\Omega_S,\Omega_V)$ would have required that p stays constant at the different view angles. Since p varied simultaneously with $e(\Omega_S,\Omega_V)$, no definite conclusions can be drawn concerning the observed angular dependency of the escape factor.

3.2. Ideal needle albedo

A non-linear, scattered relationship between BRF/ω_L and canopy BRF was observed in VIS wavelengths regardless of remote sensing data type and observation angle. Thus, an empirical fitting was performed in order to find the "ideal needle albedo" i.e. the needle

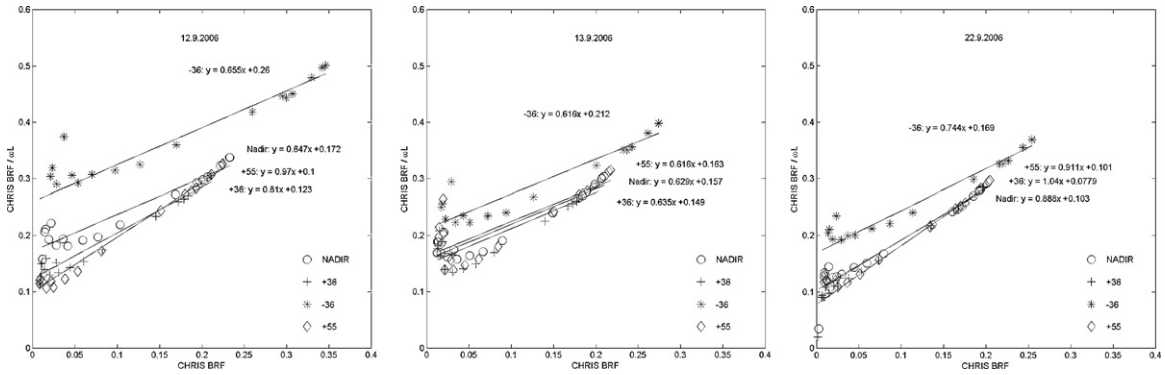

Fig. 5. BRF/ω_L vs. forest BRF relationships for three different CHRIS acquisitions (12th September, 13th September and 22nd September) and four observation angles within spectral range of 491–798 nm.

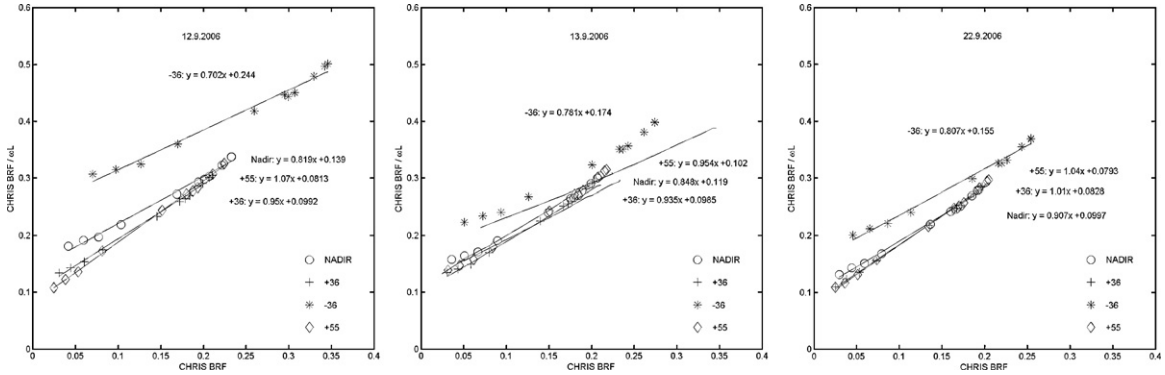

Fig. 6. BRF/ω_L vs. forest BRF relationships for three different CHRIS acquisitions (12th September, 13th September and 22nd September) and four observation angles. Spectral range limited to NIR wavelengths (707–798 nm).

Table 3
Equations of regression lines (Eq. (3)) for given CHRIS scenes and their observation angles. Both VNIR and NIR-limited spectral ranges are included. The slope of the equation corresponds to photon recollision probability and the intercept to directional escape probability.

	Acquisition 12th Sept.	Acquisition 13th Sept.	Acquisition 22nd Sept.
−36°			
VNIR range	$y = 0.655x + 0.26$	$y = 0.616x + 0.212$	$y = 0.744x + 0.169$
	$r^2 = 0.6788$	$r^2 = 0.7581$	$r^2 = 0.8306$
NIR range	$y = 0.702x + 0.244$	$y = 0.781x + 0.174$	$y = 0.807x + 0.155$
	$r^2 = 0.9854$	$r^2 = 0.9877$	$r^2 = 0.9909$
NADIR			
VNIR range	$y = 0.647x + 0.172$	$y = 0.629x + 0.157$	$y = 0.888x + 0.103$
	$r^2 = 0.8115$	$r^2 = 0.7634$	$r^2 = 0.8836$
NIR range	$y = 0.819x + 0.139$	$y = 0.848x + 0.119$	$y = 0.907x + 0.0997$
	$r^2 = 0.99$	$r^2 = 0.9921$	$r^2 = 0.9946$
+36°			
VNIR range	$y = 0.81x + 0.123$	$y = 0.635x + 0.149$	$y = 1.04x + 0.0779$
	$r^2 = 0.9081$	$r^2 = 0.6087$	$r^2 = 0.9558$
NIR range	$y = 0.95x + 0.0992$	$y = 0.935x + 0.0985$	$y = 1.01x + 0.0828$
	$r^2 = 0.9945$	$r^2 = 0.994$	$r^2 = 0.9969$
+55°			
VNIR range	$y = 0.97x + 0.1$	$y = 0.616x + 0.163$	$y = 0.911x + 0.101$
	$r^2 = 0.9447$	$r^2 = 0.4544$	$r^2 = 0.9235$
NIR range	$y = 1.07x + 0.0813$	$y = 0.954x + 0.102$	$y = 1.04x + 0.0793$
	$r^2 = 0.9962$	$r^2 = 0.9953$	$r^2 = 0.994$
VNIR range	$y = 0.618x + 0.199$	$r^2 = 0.5295$	
NIR range	$y = 0.868x + 0.139$	$r^2 = 0.9895$	

albedo that would produce a linear relationship between ω_L and canopy BRF (Eq. (5)) for the whole spectrum. The aim was to investigate how much the shape and magnitude of the so-called ideal albedo differs from the actual measured needle albedo.

An ideal needle albedo was computed for both AISA and CHRIS images acquired on 12th September 2006 (Fig. 6a). The equation of AISA regression line for NIR wavelengths (707–994 nm) and CHRIS regression for NIR wavelengths (707–994 nm) were used to invert the ideal albedo for the entire spectral region. In other words, we assumed that the relationship between canopy BRF and BRF/ω_L is perfectly linear, and analytically solved which ω_L values (i.e. ideal needle albedo values) would fulfill this assumption. The ideal albedo was similar to our measured albedo in the NIR region (Fig. 7a). In the VIS region, however, it was systematically higher

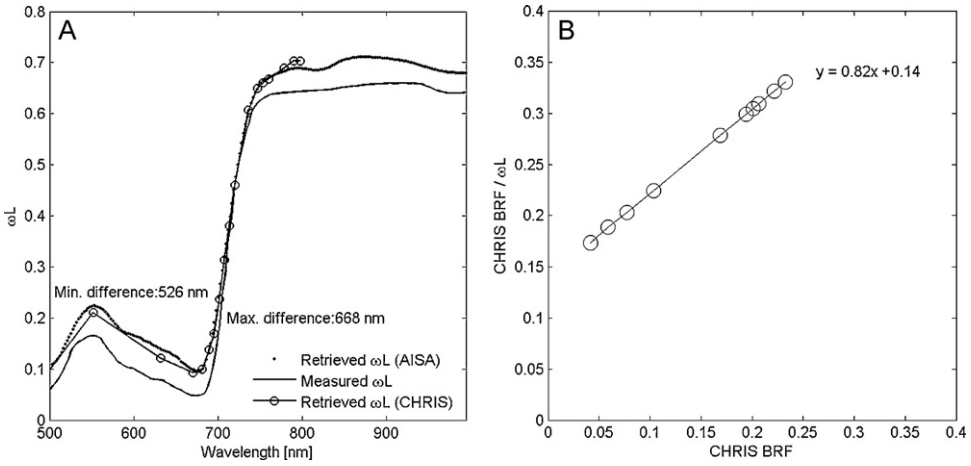

Fig. 7. (a) Comparison of measured vs. ideal albedo derived independently from AISA and NADIR CHRIS images. (b) The ideal (i.e. theoretically inverted) albedo used as input for linear retrieval regression (Eq. (2)). The RS data is a CHRIS NADIR scene acquired on September 12, 20.

than our measured needle albedo: the smallest difference was in the green region (around 500 nm), and the difference grew steadily towards the red wavelengths. The highest difference between actual measured and ideal albedo was observed at 667 nm. The ideal albedo had only shallow chlorophyll absorption features. Moreover, the largest difference between measured and theoretically derived albedos was found in the spectral region where chlorophyll a (662 nm) and chlorophyll b (642 nm) molecules exhibit strong absorption. The retrieved ideal needle albedo produced a perfectly linear relationship when used as input for stand-level retrieval of spectral invariants from the NADIR CHRIS scene from 12th September 2006 (Fig. 7b).

A challenging issue related to needle albedo is selection of proper method for scaling the leaf-level measurements up to the canopy-level while taking into the account the high variability in shaded, sunlit and transitional leaf albedos of tree crowns. In this study, we used detailed biomass, PAR and needle age class data as the basis for such upscaling. In practical applications, however, similar data may not be available and one would have to rely on general databases or typical, reference leaf albedo signatures.

The measurement of needle optical properties, especially in case of short and narrow Norway spruce needles, is a tedious task associated with a potentially higher error budget (Malenovský et al., 2006). An accurate needle albedo measurement is a crucial pre-requirement to retrieve physically accurate values of spectral invariants. The NIR part of the leaf albedo used in this study is to some extent lower when compared to needle albedo published by Williams (1991) and Huang et al. (2007). This can be explained by different needle anatomy adapted to different intensity of the incident irradiation (i.e., needles of our study were thicker in their cross-section and therefore less optically transparent in NIR). Nevertheless, the sensitivity analysis carried out for hypothetically higher NIR leaf albedo indicated insignificant influence of potential needle albedo underestimation on findings and conclusions addresses in this study (results not shown).

4. Conclusions

Based on achieved results, we can conclude with the following recommendations and suggestions for future studies and applications of the spectral invariants theory. First, our results indicated that in coniferous canopies the spectral invariants theory performs well in the NIR domain. This suggests that the spectral invariants theory could be a powerful tool for modeling the relationship between canopy structure and reflectance in wavelengths where multiple scattering is high (i.e. the NIR domain). This presents an important progress in modeling canopy scattering, because describing multiple scattering has been problematic in previous geometric-optical forest reflectance models. The VIS domain, on the other hand, seems to be unsuitable for applying the spectral invariants theory due to the high absorption by the foliar pigments limiting multiple scattering and recollision rates. Secondly, the results suggest that retrieval of the escape factor could be used as a new method to describe the BRDF of a canopy. By theory, the escape factor provides more useful information about a canopy than simply the escape probability: the escape factor is the highest in backscattering directions and the lowest in forward scattering directions, and it might be used as a proxy of the canopy BRDF shape. The observed behavior of the escape factor is in line with the theory, but the retrieval algorithm produced certain angular dependency in the estimated recollision probability. A more robust retrieval algorithm would be needed to produce more consistent estimates of the escape factor.

Acknowledgements

We thank Ivana Tomášková for information on Bílý Kříž forest stand variables, Jan Hanuš for AISA image data processing, and Lucie Homolová with Lucia Yanez Rausell for preprocessing of needle optical data. This article is an output of the CzechGlobe – Centre, that is being developed within OP RDI and co-financed from EU funds and state budget of the Czech Republic (Project: Czech Globe Centre for Global Climate Change Impacts Studies, Reg. No. CZ.1.05/1.1.00/02.0073). This study was funded by the Ministry of the Environment of the Czech Republic (ForChange SP/2d1/70/08 (MŽP) project), Emil Aaltonen Foundation, University of Helsinki Research Funds and the Academy of Finland.

References

Daughtry, C.S.T., Biehl, L.L., Ranson, K.J., 1989. A new technique to measure the spectral properties of conifer needles. Remote Sensing of Environment 27, 81–91.
Ganguly, S., Schull, M.A., Samanta, A., Shabanov, N.V., Milesi, C., Nemani, R.R., et al., 2008a. Generating vegetation leaf area index earth system data record from multiple sensors. Part 1. Theory. Remote Sensing of Environment 112, 4333–4343.
Ganguly, S., Samanta, A., Schull, M.A., Shabanov, N.V., Milesi, C., Nemani, R.R., et al., 2008b. Generating vegetation leaf area index Earth system data record from multiple sensors. Part 2. Implementation, analysis and validation. Remote Sensing of Environment 112, 4318–4332.
Huang, D., Knyazikhin, Y., Dickinson, R.E., Rautiainen, M., Stenberg, P., Disney, M., et al., 2007. Canopy spectral invariants for remote sensing and model applications. Remote Sensing of Environment 106, 106–122.
Huang, D., Knyazikhin, Y., Wang, W., Deering, D.W., Stenberg, P., Shabanov, N., et al., 2008. Stochastic transport theory for investigating the three-dimensional canopy structure from space measurements. Remote Sensing of Environment 112, 35–50.

Knyazhikin, Y., Schull, M.A., Xu, L., Myneni, R., Samanta, A., 2011. Canopy spectral invariants. Part 1. A new concept in remote sensing of vegetation. Journal of Quantitative Spectroscopy and Radiative Transfer 112, 727–735.

Kratochvilová, I., Janouš, D., Marek, M., Barták, M., Říha, L., 1989. Production activity of mountain cultivated Norway spruce stands under the impact of air pollution. Ekologia 8 (*4*), 407–419.

Lewis, P., Disney, M., 2007. Spectral invariants and scattering across multiple scales from within-leaf to canopy. Remote Sensing of Environment 109 (2), 196–206.

Malenovský, Z., Albrechtová, J., Lhotáková, Z., Zurita-Milla, R., Clevers, J.G.P.W., Schaepman, M.E., et al., 2006. Applicability of the PROSPECT model for Norway spruce needles. International Journal of Remote Sensing 27 (24), 5315–5340.

Mesarch, M.A., Walter-Shea, E.A., Asner, G.P., Middleton, E.M., Chan, S.S., 1999. A revised measurement methodology for conifer needles spectral optical properties: evaluating the influence of gaps between elements. Remote Sensing of Environment 68, 177–192.

Mõttus, M., Stenberg, P., 2008. A simple parameterization of canopy reflectance using photon recollision probability. Remote Sensing of Environment 112, 1545–1551.

Mõttus, M., 2007. Photon recollision probability in discrete crown canopies. Remote Sensing of Environment 110, 176–185.

Mõttus, M., Stenberg, P., Rautiainen, M., 2007. Photon recollision probability in heterogeneous forest canopies: compatibility with a hybrid GO model. Journal of Geophysical Research - Atmospheres 112 (D03104), doi:10.1029/2006JD007445.

Oak Ridge National Laboratory Distributed Active Archive Center (ORNL DAAC), 2005. Oak Ridge National Laboratory Distributed Active Archive Center (ORNL DAAC), FLUXNET A Global Network Integrating Worldwide CO_2 Flux Measurements Web page available on-line on http://www.fluxnet.ornl.gov/fluxnet/index.cfm (2005) Oak Ridge, Tennessee, USA, Accessed November 30, 2005.

Pokorný, R., 2002. Index listové plochy v porostech lesních dřevin (Needle area index of forest stands). Faculty of Forestry and Wood Technology Mendel, University of Agriculture and Forestry, Brno (PhD. thesis, Czech), pp. 135.

Pokorný, R., Tomášková, I., Havránková, K., 2008. Temporal variation and efficiency of needle area index in young mountain Norway spruce stand. European Journal of Forest Research 127, 359–367.

Rautiainen, M., Stenberg, P., 2005. Application of photon recollision probability in coniferous canopy reflectance simulations. Remote Sensing of Environment 96, 98–107.

Rautiainen, M., Mõttus, M., Stenberg, P., 2009. On the relationship of canopy LAI and photon recollision probability in boreal forests. Remote Sensing of Environment 113, 458–461.

Schaepman, M., Ustin, S., Plaza, A., Painter, T., Verrelst, J., Liang, S., 2009. Earth system science related imaging spectroscopy—an assessment. Remote Sensing of Environment 113, S123–S137.

Schull, M.A., Ganguly, S., Samanta, A., Huang, D., Shabanov, N.V., Jenkins, J.P., et al., 2007. Physical interpretation of the correlation between multi-angle spectral data and canopy height. Geophysical Research Letters 34 (L18405), doi:10.1029/2007GL031143.

Schull, M.A., Knyazikhin, Y., Xu, L., Samanta, A., Carmona, P.L., Lepine, L., et al., 2011. Canopy spectral invariants. Part 2. Application to classification of forest types from hyperspectral data. Journal of Quantitative Spectroscopy and Radiative Transfer 112, 736–750.

Smolander, S., Stenberg, P., 2005. Simple parameterizations for the radiation budget of uniform broadleaved and coniferous canopies. Remote Sensing of Environment 94, 355–363.

Stenberg, P., 2007. Simple analytical formula for calculating average photon recollision probability in vegetation canopies. Remote Sensing of Environment 109 (2), 221–224.

Urban, O., Janouš, D., Acosta, M., Czerný, R., Marková, I., Navrátil, M., et al., 2007. Ecophysiological controls over the net ecosystem exchange of mountain spruce stand. Comparison of the response in direct vs. diffuse solar radiation. Global Change Biology 13, 157–168.

Widlowski, J.-L., Taberner, M., Pinty, B., Bruniquel-Pinel, V., Disney, M., Fernandes, R., et al., 2007. Third Radiation Transfer Model Intercomparison (RAMI) exercise: documenting progress in canopy reflectance models. Journal of Geophysical Research 112 (D09111), doi:10.1029/2006JD007821.

Williams, D.L., 1991. A comparison of spectral reflectance properties at the needle, branch and canopy level for selected conifer species. Remote Sensing of Environment 35, 79–93.